

Deep Gated Recurrent and Convolutional Network Hybrid Model for Univariate Time Series Classification

Nelly Elsayed, *Student Member, IEEE*, Anthony S. Maida and Magdy Bayoumi, *Life Fellow, IEEE*

Abstract—Hybrid LSTM-fully convolutional networks (LSTM-FCN) for time series classification have produced state-of-the-art classification results on univariate time series. We show that replacing the LSTM with a gated recurrent unit (GRU) to create a GRU-fully convolutional network hybrid model (GRU-FCN) can offer even better performance on many time series datasets. The proposed GRU-FCN model outperforms state-of-the-art classification performance in many univariate time series datasets without additional supporting algorithms requirement. Furthermore, since the GRU uses a simpler architecture than the LSTM, it has fewer training parameters, less training time, smaller memory storage requirement, and a simpler hardware implementation, compared to the LSTM-based models.

Index Terms—GRU-FCN, LSTM, fully convolutional neural network, time series, classification

I. INTRODUCTION

A time series (TS) is a sequence of data points obtained at successive equally-spaced time points, ordinarily in a uniform interval time domain [1]. TSs are used in several research and industrial fields where temporal analysis measurements are involved such as in signal processing [2], pattern recognition [3], mathematics [1], psychological and physiological signals analysis [4], [5], earthquake prediction [6], weather readings [7], and statistics [1]. There are two types of time series: univariate and multivariate. In this paper, we study the univariate time series classification.

There are many approaches to time series classification. The distance-based classifier based on the k-nearest neighbor (KNN) algorithm is considered a baseline technique for time series classification. Mostly, distance-based classifier uses Euclidean or Dynamic Time Warping (DTW) as a distance measure [8]. Feature-based time series classifiers are also widely used such as the bag-of-SFA-symbols (BOSS) [9] and the bag-of-features framework (TSBF) [10] classifiers. Ensemble-based classifiers combine separate classifiers into one model to reach a higher classification accuracy such as the elastic ensemble (PROP) [11], and the collective of transform-based ensemble (COTE) [12] classifiers.

Convolutional neural network (CNN) based classifiers have advantages over other classification methods because CNNs provide the classifier with a preprocessing mechanism within the model. Examples are the multi-channel CNN (MC-CNN) classifier [13], the multi-layered perceptron (MLP) [4], the fully convolutional network (FCN) [4] and, specifically, the residual network (ResNet) [4].

The present paper focuses on the recurrent neural network based classification approaches such as LSTM-FCN [5]

TABLE I: Comparison of GRU and LSTM Computational Elements.

Comparison	LSTM	GRU
number of gates	3	2
number of activations	2	1
state memory cell	Yes	No
number of weight matrices	8	6
number of bias vectors	3	4
number of elementwise multiplies	3	3
number of matrix multiplies	8	6

and ALSTM-FCN [5]. These models combine both temporal CNNs and long short-term memory (LSTM) models to provide the classifier with both feature extraction and time dependencies through the dataset during the classification process. These models use additional support algorithms such as attention and fine-tuning algorithms to enhance the LSTM learning due to its complex structure and data requirements.

This paper studies whether the use of gated-recurrent units (GRUs) can improve the hybrid classifiers listed above. We create the GRU-FCN by replacing the LSTM with a GRU in the LSTM-FCN [5]. We intentionally kept the other components of the entire model without changes to make an empirical comparison between the LSTM and GRU in a same model structure to obtain a fair comparison between both architectures regarding the univariate time series classification task. Like the LSTM-FCN, our model does not require feature engineering or data preprocessing before the training or testing stages. The GRU is able to learn the temporal dependencies within the dataset. Moreover, the GRU has a smaller block architecture and shows comparable performance to the LSTM without need for additional algorithms to support the model.

Although it is difficult to determine the best classifier for all time series types, the proposed model seeks to achieve equivalent accuracy to state-of-the-art classification models in univariate time series classification. Following [4] and [5], our tests use the UCR time series classification archive benchmark [14] to compare our model with other state-of-the-art univariate time series classification models. Our model achieved higher classification performance on several datasets compared to other state-of-the-art classification models.

II. MODEL COMPONENTS

A. Gated Recurrent Unit (GRU)

The gated recurrent unit (GRU) was introduced in [15] as another type of gate-based recurrent unit which has a

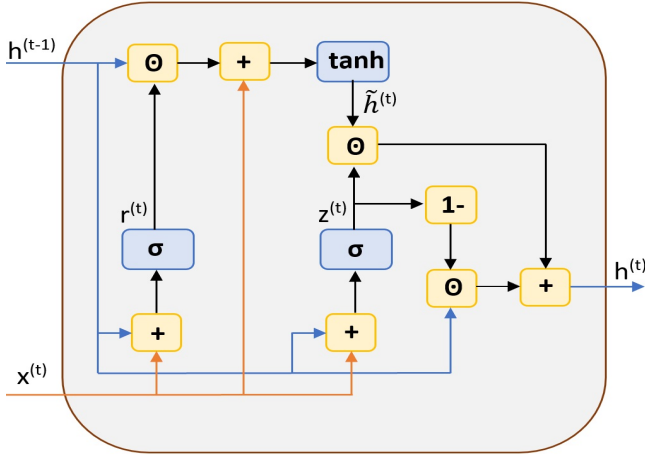


Fig. 1: Block architecture for an unrolled GRU.

smaller architecture and comparable performance to the LSTM unit. The GRU consists of two gates: reset and update. The architecture of an unrolled GRU block is shown in Figure. 1. $r^{(t)}$ and $z^{(t)}$ denote the values of the reset and update gates at time step t , respectively. $x_i \in \mathbb{R}^n$ is a 1D input vector to the GRU block at time step t . $\tilde{h}^{(t)}$ is the output candidate of the GRU block. $h^{(t-1)}$ is the recurrent GRU block output of time step $t-1$ and the current output at time t is $h^{(t)}$. Assuming a one-layer GRU, the reset gate, update gate, output candidate, and GRU output are calculated as follows [15]:

$$z^{(t)} = \sigma(W_{zx}x^{(t)} + U_{zh}h^{(t-1)} + b_z) \quad (1)$$

$$r^{(t)} = \sigma(W_{rx}x^{(t)} + U_{rh}h^{(t-1)} + b_r) \quad (2)$$

$$\tilde{h}^{(t)} = \tanh(W_x x^{(t)} + U_h(r^{(t)} \odot h^{(t-1)} + b)) \quad (3)$$

$$h^{(t)} = (1 - z^{(t)}) \odot h^{(t-1)} + z^{(t)} \odot \tilde{h}^{(t)} \quad (4)$$

Where W_{zx} , W_{rx} , and W_x are the feedforward weights and U_{hz} , U_{hr} , and U_h are the recurrent weights of the update gate, reset gate, and output candidate activation respectively. b_z , b_r and b are the biases of the update gate, reset gate and the output candidate activation $\tilde{h}^{(t)}$, respectively. Figure 3 shows the GRU architecture with weights and biases made explicit.

Like the RNN and LSTM, the GRU models temporal (sequential) datasets. The GRU uses its previous time step output and current input to calculate the next output. The GRU has the advantage of smaller size over the LSTM. The GRU consists of two gates (reset and update), while the LSTM has three gates: input, output and forget. The GRU has one unit activation, but the LSTM has two unit activations: input-update and output activations. Also, the GRU does not contain the memory state cell which exists in the LSTM model. Thus, the GRU requires fewer trainable parameters, and shorter training time compared to the LSTM. Table I compares GRU and LSTM architecture components.

B. Temporal Convolutional Neural Network

The Convolutional Neural Network (CNN), introduced in 1989 [16], utilizes weight sharing over grid-structured datasets such as images and time series [17], [18]. The convolutional

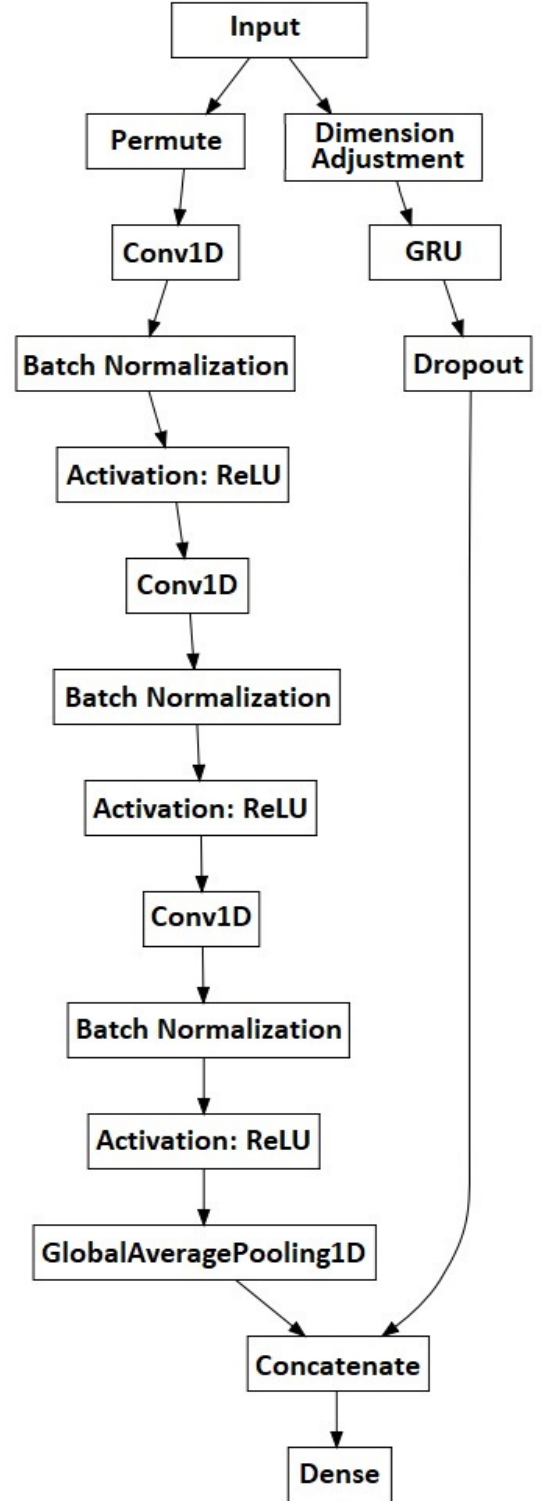


Fig. 2: The proposed GRU-FCN model architecture diagram rendered using the Keras visualization tool and modified from [4], [5] architectures.

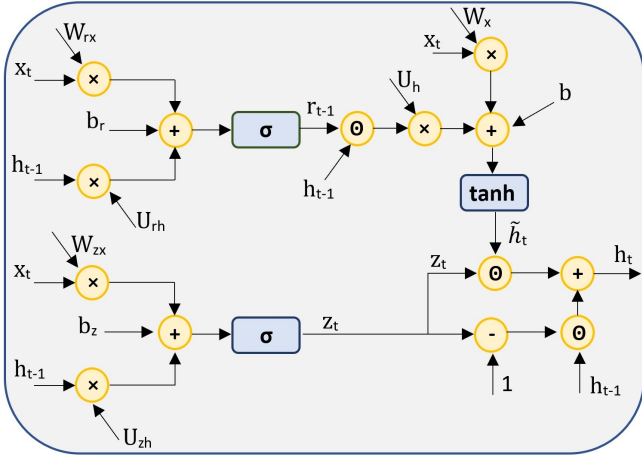


Fig. 3: The GRU architecture showing the weights of each component.

layers within the CNN learn to extract complex feature representations from the data with little or no preprocessing. The temporal FCN consists of many layers of convolutional blocks that may have different or same kernel sizes, followed by a dense layer softmax classifier [18]. For time series problems, the values of each convolutional block in the FCN, are calculated as follows [4]:

$$y_i = W_i * x_i + b_i \quad (5)$$

$$z_i = BN(y) \quad (6)$$

$$out_i = ReLU(z) \quad (7)$$

where $x_i \in \mathbb{R}^n$ is a 1D input vector which represents a time series segment, W_i is the 1D convolutional kernel of weights, b_i is the bias, and y is the output vector of the convolutional block i . z_i is the intermediate result after applying batch normalization [19] on the convolutional block which then is passed to the rectified linear unit $ReLU$ [20] to calculate the output of the convolutional layer out_i .

III. MODEL ARCHITECTURE

As stated in the introduction, our model replaces the LSTM with a GRU in a hybrid gated-FCN. We intentionally did not change the other components of the entire model to attain a fair comparison between GRU and LSTM architectures in the same model structure for univariate time series classification. Our model is based on the framework introduced in [4], [5]. The proposed architecture actual implementation is shown in Figure 2. The architecture has two parallel parts: a GRU and a temporal FCN. Our model uses three layers FCN architecture proposed in [4]. The dimension adjustment aims to change the dimensions of the input to be compatible with the GRU recurrent design [21]. We also used the global average pooling layer [22] to interpret the classes and to reduce the number of trainable parameters comparing to the fully connected layer, without any sacrifice in the accuracy. The FCN 1D kernel numbers are 128, 256, and 128 with kernel sizes 8, 5, and 3 in each convolutional layer, respectively. The weights were initialized using the He uniform variance

scaling initializer [23]. In addition, we used the GRU instead of LSTMs that were used in [5] models to reduce the number of trainable parameters, memory, and training time. Moreover, we removed the masking and any extra supporting algorithms such as an attention mechanism, and fine-tuning that were used in the LSTM-FCN and ALSTM-FCN models [5]. The GRU is unfolded by eight unfolds as used in [5] for univariate time series. The hyperbolic tangent (\tanh) function used as the unit activation and the hard-sigmoid ($hardSig$) function [24] is used as the recurrent activation (gate activation) of the GRU architecture. The weights were initialized using the *glorot_uniform* initializer [25], [26] and the biases were initialized to zero. The input was fitted using the concept used in [5] to fit an input to a recurrent unit. We used the Adam optimization function [27] with $\beta_1 = 0.9$, $\beta_2 = 0.999$ and initial learning rate $\alpha = 0.01$. The learning rate α was reduced by a factor of 0.8 every 100 training steps until it reached the minimum rate $\alpha = 0.0001$. The dense layer uses the softmax classifier [28] using the categorical crossentropy loss function [18]. In this paper our goal is to make a fair comparison between the LSTM-based model and our GRU-based model. Thus, we used the same number of epochs that was assigned by the original LSTM-FCN model [5] for each univariate time series. The number of epochs that we assigned for each dataset used is shown in Table II .

The input to the model is the raw dataset without applying any normalizations or feature engineering prior to the training process. The FCN is responsible for feature extraction from the time series [4] and the GRU enables the model to learn temporal dependencies within the time series. Therefore the model learns both the features and temporal dependencies to predict the correct class for each training example.

IV. METHOD AND RESULTS

We implemented our model by modifying the original LSTM-FCN [5]. We found that the fine-tuning algorithm has not been applied in the actual LSTM-FCN and ALSTM-FCN implementation on source code github which shared by the authors [5] and mentioned in their literature. In addition, the LSTM-FCN [5] authors used a permutation algorithm for fitting the input to the FCN part which was not mentioned in their literature. Therefore, we generated the actual LSTM-FCN and ALSTM-FCN implementations to record the results based on their actual code implementation. In addition, to record their training time, memory requirement, number of parameters and f1-score. The Keras API [26] with TensorFlow backend [29] were used in the implementation of the LSTM-FCN, ALSTM-FCN and GRU-FCN models. The source code of our GRU-FCN implementation can be found on github: <https://github.com/NellyElsayed/GRU-FCN-model-for-univariate-time-series-classification>.

We tested our model on the UCR time series archive [14] as one of the standard benchmarks for time series classification. Each dataset is divided into training and testing sets. The number of classes in each time series, the length and the size of both the training and test sets are shown in Table II based on the datasets description in [14]. The UCR benchmark datasets

TABLE II: The UCR datasets descriptions based on [14] and their experimental adjustments used in the GRU-FCN implementation.

Dataset	Type	# Classes	Length	Train size	Test size	# epochs	Train Batch	Test Batch
Adiac	Image	37	176	390	391	4000	128	128
ArrowHead	Image	3	251	36	175	4000	32	128
Beef	Spectro	5	470	30	30	8000	64	64
BeetleFly	Image	2	512	20	20	8000	64	64
BirdChicken	Image	2	512	20	20	8000	64	64
Car	Sensor	4	577	60	60	2000	128	128
CBF	Simulated	3	128	30	900	2000	32	128
ChlorineConc	Sensor	3	166	467	3840	2000	128	128
CinCECGTorso	Sensor	4	1639	40	1380	500	128	128
Coffee	Spectro	2	286	28	28	500	64	64
Computers	Device	2	720	250	250	2000	128	128
CricketX	Motion	12	300	390	390	2000	128	128
CricketY	Motion	12	300	390	390	2000	128	128
CricketZ	Motion	12	300	390	390	2000	64	128
DiatomSizeR	Image	4	345	16	306	2000	64	64
DisPhOAgeGrp	Image	3	80	400	139	2000	128	128
DisPhOCorrect	Image	2	80	600	276	2000	128	128
DisPhTW	Image	6	80	400	139	2000	128	128
Earthquakes	Sensor	2	512	322	139	2000	128	128
ECG200	ECG	2	96	100	100	8000	64	64
ECG5000	ECG	5	140	500	4500	2000	128	128
ECGFiveDays	ECG	2	136	23	861	2000	128	128
ElectricDevices	Device	7	96	8926	7711	2000	128	128
FaceAll	Image	14	131	560	1690	2000	128	128
FaceFour	Image	4	350	24	88	2000	128	128
FacesUCR	Image	14	131	200	2050	2000	128	128
FiftyWords	Image	50	270	450	455	2000	128	128
Fish	Image	7	463	175	175	2000	128	128
FordA	Sensor	2	500	3601	1320	2000	128	128
FordB	Sensor	2	500	3636	810	1600	128	128
GunPoint	Motion	2	150	50	150	2000	128	128
Ham	Spectro	2	431	109	105	2000	128	128
HandOutlines	Image	2	2709	1000	370	2000	64	128
Haptics	Motion	5	1092	155	308	2000	128	128
Herring	Image	2	512	64	64	2000	128	128
InlineSkate	Motion	7	1882	100	550	2000	128	128
InsWingSound	Sensor	11	256	220	1980	1000	128	128
ItalyPowD	Sensor	2	24	67	1029	2000	64	128
LargeKApp	Device	3	720	375	375	2000	128	128
Lightning2	Sensor	2	637	60	61	4000	128	128
Lightning7	Sensor	7	319	70	73	3000	32	32
Mallat	Simulated	8	1024	55	2345	2500	128	128
Meat	Spectro	3	448	60	60	2000	64	128
MedicalImages	Image	10	99	381	760	2000	64	128
MidPhOAgeGrp	Image	3	80	400	154	2000	128	128
MidPhOCorrect	Image	2	80	600	291	2000	128	128
MidPhTW	Image	6	80	399	154	2000	128	128
MoteStrain	Sensor	2	84	20	1252	2000	128	128
NonInvECGTh1	ECG	42	750	1800	1965	2000	128	128
NonInvECGTh2	ECG	42	750	1800	1965	2000	128	128
OliveOil	Spectro	4	570	30	30	6000	64	128
OSULeaf	Image	6	427	200	242	2000	64	128
PhalOCorrect	Image	2	80	1800	858	2000	64	128
Phoneme	Sensor	39	1024	214	1896	2000	64	128
Plane	Sensor	7	144	105	105	200	16	16
ProxPhOAgeGrp	Image	3	80	400	205	2000	128	128
ProxPhOCorrect	Image	2	80	600	291	2000	128	128
ProxPhTW	Image	6	80	400	205	2000	128	128
RefDevices	Device	3	720	375	375	2000	64	64
ScreenType	Device	3	720	375	375	2000	64	128
ShapeletSim	Simulated	2	500	20	180	2000	128	128
ShapesAll	Image	60	512	600	600	4000	64	64
SmlKitApp	Device	3	720	375	375	2000	128	64
SonyAIBORI	Sensor	2	70	20	601	2000	64	128
SonyAIBORII	Sensor	2	65	27	953	2000	64	128
StarLightCurves	Sensor	3	1024	1000	8236	2000	64	64
Strawberry	Spectro	2	235	613	370	8000	64	64
SwedishLeaf	Image	15	128	500	625	8000	64	64
Symbols	Image	6	398	25	995	2000	64	64
SynControl	Simulated	6	60	300	300	4000	16	128
ToeSegI	Motion	2	277	40	228	2000	128	64
ToeSegII	Motion	2	343	36	130	2000	128	32
Trace	Sensor	4	275	100	100	1000	64	128
TwoLeadECG	ECG	2	82	23	1139	2000	64	64
TwoPatterns	Simulated	4	128	1000	4000	2000	32	128
UWaveAll	Motion	8	945	896	3582	500	16	16
UWaveX	Motion	8	315	896	3582	2000	64	16
UWaveY	Motion	8	315	896	3582	2000	64	64
UWaveZ	Motion	8	315	896	3582	2000	64	64
Wafer	Sensor	2	152	1000	6164	1500	64	64
Wine	Spectro	2	234	57	54	8000	64	64
WordSynonyms	Image	25	270	267	638	1500	64	64
Worms	Motion	5	900	181	77	2000	64	64
WormsTwoClass	Motion	2	900	181	77	1000	16	16
Yoga	Image	2	426	300	3000	1000	128	128

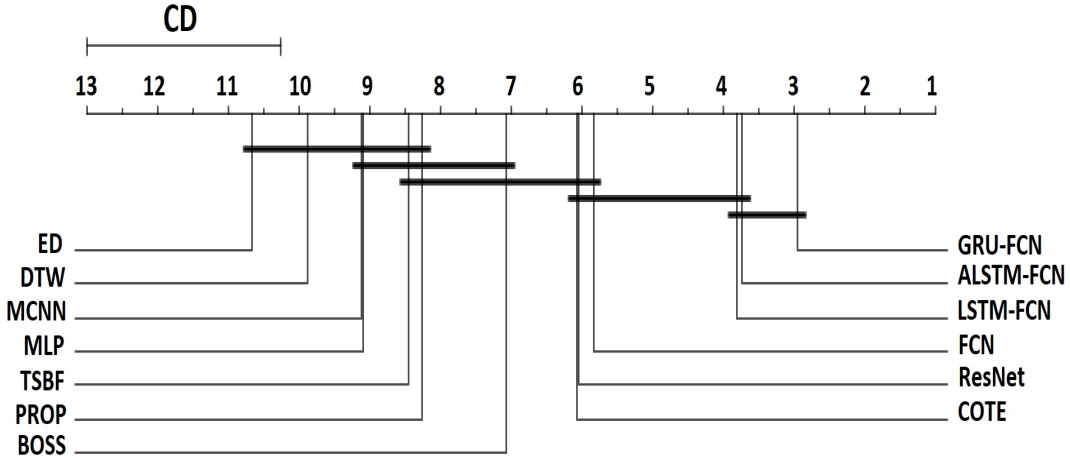


Fig. 4: Critical difference diagram based on arithmetic mean of model ranks.

have different types of collected sources: 29 datasets of image source, 6 spectro source, 5 simulated source, 19 sensor source, 6 device source, 12 motion source, and 6 electrocardiogram (ECG) source. In addition, as we mentioned in the previous Section, Table II also shows the number of epochs through training, and the batch sizes of the training and testing stages based on our experiments.

We compared our GRU-FCN with several state-of-the-art time series methods that also were studied in [4] and [5]. These included FCN [4] which is based on a fully convolutional network, LSTM-FCN [5], ALSTM-FCN [5], that are based on long short-term memory and fully convolutional networks, ResNet [4] which based on convolutional residual networks, multi-scale convolution neural networks model (MCNN) [13], multi-layered perceptrons model (MLP) [4], collective of transformation-based ensembles model (COTE) [12] which based on transformation ensembles, dynamic time warping model (DTW) [30] that is based on a weighted dynamic time warping mechanism, PROP model [11] which is based on elastic distance measures, BOSS model [9] that based on noise reduction in the time series representation, time series based on a bag-of-features representation (TSBF) model [10], and Euclidean distance (ED) model [14]. Our model shows the overall highest number of being the best classifier for 39 time series out of 85. Our model also shows the overall smallest classification error, arithmetic average rank, and mean per-class classification error (MPCE) compared to the other models as shown in Table III.

Table IV shows a comparison between the number of parameters, training time and memory required to save the trainable weights of the GRU-FCN and both LSTM-FCN and ALSTM-FCN models as the existing LSTM-based to-date univariate classification models over the UCR 85 datasets. The GRU-FCN has smaller number of parameters for all the datasets. The GRU-FCN saves overall 1207KB, and 5719KB memory requirements to save the trained model's weight; and 106.065, and 62.271 minutes to train the models over the UCR datasets comparing to the LSTM-FCN and ALSTM-FCN, respectively. Therefore, the GRU-FCN is preferable as low budget classification model with high accuracy performance.

We evaluated our model using the Mean Per-Class Error (MPCE) used in [4] to evaluate performance of a classification method over multiple datasets. The MPCE for a given model is calculated based on the per-class error (PCE) as follows:

$$PCE_m = \frac{e_m}{c_m} \quad (8)$$

$$MPCE = \frac{1}{M} \sum_{m=1}^M PCE_m \quad (9)$$

where e_m is the error rate for dataset m consisting of c_m classes. M is the number of tested datasets.

Table III shows the MPCE value for our GRU-FCN and other state-of-the-art models on the UCR benchmark datasets [14]. The results obtained by implementing GRU-FCN and generating LSTM-FCN, and ALSTM models based on their actual implementation on github. For the other models, we obtained the results from their own publications. Our GRU-FCN has the smallest MPCE value compared to the other state-of-the-art classification models. This means that generally our GRU-FCN model performance across the different datasets is higher than the other state-of-the-art models.

Figures 5, 6, 7, 8 are showing the loss value of both the training and validation processed of datasets. Each of these figures represents the loss process over image, motion, simulated, and source-obtained datasets from the UCR benchmark datasets respectively. These figures show that the average difference between the training and validation loss for the GRU-FCN is smaller that the LSTM-FCN and ALSTM-FCN models.

Table V shows the f1-score (also known as F-score or F-measure) [31], [32] for GRU-FCN, LSTM-FCN, and ALSTM-FCN classifiers. The f1-score shows the overall measure of a model's accuracy over each dataset used. The f1-score measuring based on both the precision and recall values of the classification model [31], [32]. The f1-score is calculated as follows [31], [32]:

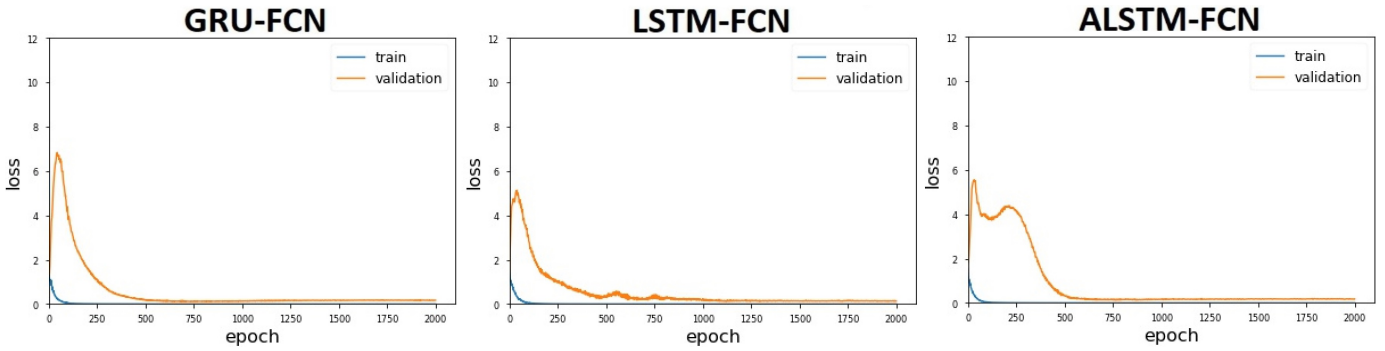


Fig. 5: The loss value of GRU-FCN, LSTM-FCN, and ALSTM-FCN models over the image-source obtained (DiatomSizeR dataset) training and validation processes.

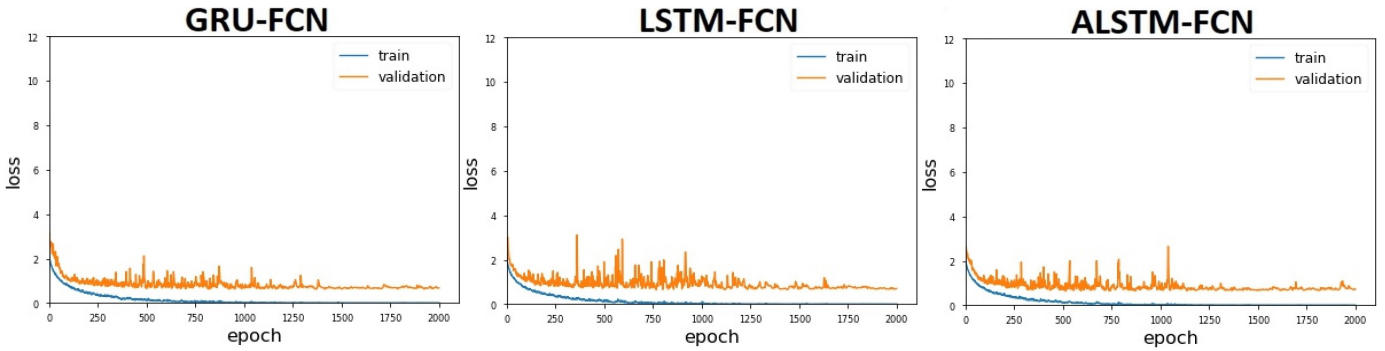


Fig. 6: The loss value of GRU-FCN, LSTM-FCN, and ALSTM-FCN models over the motion-source obtained (CricketX dataset) training and validation processes.

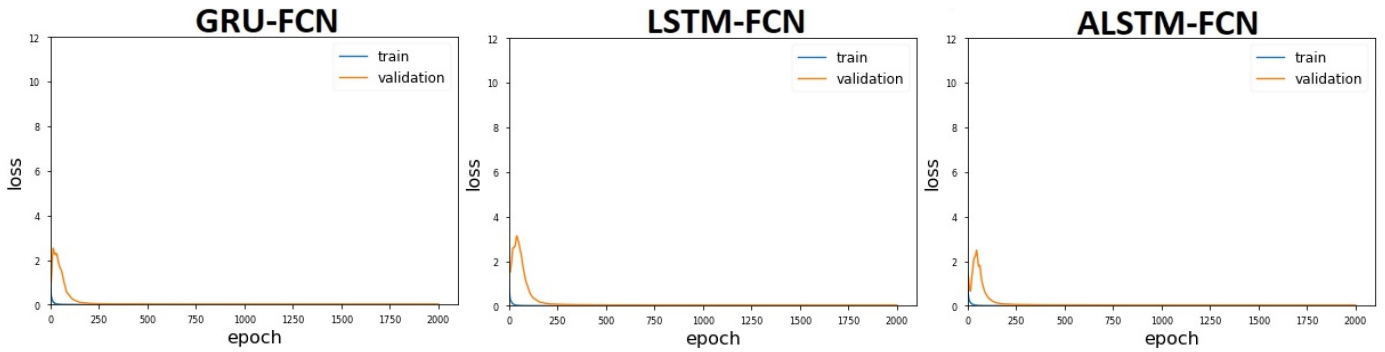


Fig. 7: The loss value of GRU-FCN, LSTM-FCN, and ALSTM-FCN models over the simulated-source obtained (CDF dataset) training and validation processes.

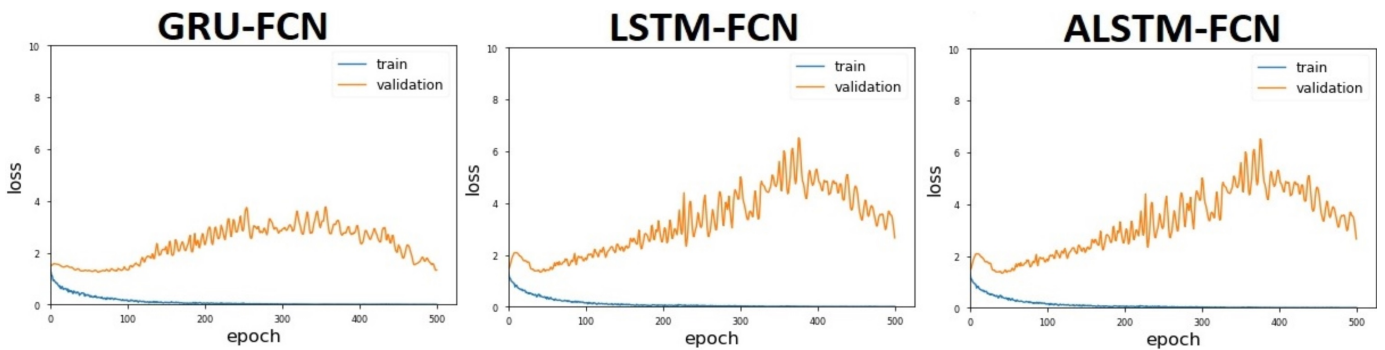


Fig. 8: The loss value of GRU-FCN, LSTM-FCN, and ALSTM-FCN models over the sensor-source obtained (ChlorineCon dataset) training and validation processes.

TABLE V: The f1-score value of the proposed GRU-FCN model and the LSTM-based architectures over the UCR benchmark datasets [14].

Dataset	f1-Score		
	GRU-FCN	LSTM-FCN	ALSTM-FCN
Adiac	0.795	0.770	0.780
ArrowHead	0.711	0.694	0.695
Beef	0.819	0.873	0.765
BeetleFly	1.0	1.0	0.949
BirdChicken	1.0	1.0	1.0
Car	0.954	0.952	0.947
CBF	0.995	0.994	0.989
ChlorineCon	0.766	0.791	0.767
CinCECGTorso	0.379	0.321	0.375
Coffee	1.0	1.0	1.0
Computers	0.916	0.914	0.913
CricketX	0.786	0.782	0.784
CricketY	0.756	0.786	0.776
CricketZ	0.779	0.778	0.761
DiatomSizeR	0.926	0.926	0.935
DisPhOAgeGrp	0.645	0.614	0.636
DisPhOCorrect	0.813	0.804	0.813
DisPhTW	0.477	0.469	0.479
Earthquakes	0.483	0.466	0.466
ECG200	0.910	0.900	0.909
ECG5000	0.253	0.251	0.263
ECGFiveDays	0.991	0.991	0.991
ElectricDevices	0.195	0.196	0.197
FaceAll	0.137	0.134	0.136
FaceFour	0.960	0.949	0.949
FacesUCR	0.892	0.898	0.896
50words	0.353	0.330	0.353
Fish	0.962	0.964	0.957
FordA	0.926	0.928	0.928
FordB	0.928	0.930	0.929
GunPoint	1.0	1.0	1.0
Ham	0.788	0.788	0.770
HandOutlines	0.875	0.873	0.866
Haptics	0.528	0.523	0.515
Herring	0.717	0.722	0.694
InlineSkate	0.454	0.474	0.446
InWingSound	0.477	0.432	0.410
ItalyPower	0.970	0.970	0.972
LargeKApp	0.406	0.407	0.410
Lightning2	0.765	0.767	0.767
Lightning7	0.872	0.833	0.858
MALLAT	0.971	0.970	0.971
Meat	0.925	0.870	0.973
MedicalImages	0.714	0.686	0.701
MidPhOutlineAgeGrp	0.507	0.347	0.445
MidPhOCorrect	0.823	0.821	0.819
MidPhTW	0.329	0.314	0.320
MoteStrain	0.925	0.920	0.915
NonInvECGTh1	0.911	0.908	0.905
NonInvECGTh2	0.899	0.896	0.894
OliveOil	0.853	0.611	0.885
OSULeaf	0.988	0.979	0.988
PhalOCorrect	0.812	0.803	0.809
Phoneme	0.025	0.026	0.026
Plane	0.888	0.888	0.882
ProxPhOeAgeGrp	0.600	0.594	0.436
ProxPhOCorrect	0.896	0.904	0.896
ProxPhTW	0.545	0.504	0.469
RefDevices	0.277	0.241	0.241
ScreenType	0.297	0.302	0.308
ShapeletSim	0.842	0.842	0.842
ShapesAll	0.108	0.108	0.107
SmlKitApp	0.345	0.361	0.370
SonyAIBORI	0.984	0.974	0.983
SonyAIBORII	0.980	0.978	0.977
StarLightCurves	0.975	0.961	0.962
Strawberry	0.818	0.818	0.818
SwedishLeaf	0.807	0.801	0.811
Symbols	0.980	0.982	0.974
SynControl	0.522	0.516	0.511
ToeSeg1	0.708	0.746	0.746
ToeSeg2	0.582	0.563	0.577
Trace	1.0	0.986	0.983
TwoLeadECG	0.999	0.999	0.999
TwoPatterns	0.986	0.989	0.971
UWaveAll	0.782	0.766	0.754
UWaveX	0.665	0.654	0.659
UWaveY	0.698	0.695	0.686
UWaveZ	0.736	0.739	0.743
Wafer	0.996	0.996	0.996
Wine	0.887	0.887	0.887
WordSynonyms	0.380	0.327	0.345
Worms	0.448	0.423	0.425
WormsTwoClass	0.530	0.525	0.542
Yoga	0.882	0.906	0.914

$$precision = \frac{TP}{TP + FP} \quad (10)$$

$$recall = \frac{TP}{TP + FN} \quad (11)$$

$$f1-score = 2 \times \frac{precision \times recall}{precision + recall} \quad (12)$$

where TP, FP, FN stands for true-positive, false-positive and false-negative respectively. The GRU-FCN shows the highest f1-score for 53 out of 85 datasets comparing to the LSTM-FCN and ALSTM-FCN that both of these models have the highest f1-score for only 29 out of 85 datasets.

Figure 4 shows the critical difference diagram [33] for Nemenyi or Bonferroni-Dunn test [34] with $\alpha = 0.05$ on our GRU-FCN and the state-of-the-art models based on the ranks arithmetic mean on the UCR benchmark datasets. This graph shows the significant classification accuracy improvement of our GRU-FCN compared to the other state-of-the-art models.

The Wilcoxon signed-rank test is one of substantial tests to provide the classification method efficiency [35], [36]. Table VI shows the Wilcoxon signed-rank test [35], [37] among the twelve state-of-the-art classification models. This provides the overall accuracy evidence of each of the twelve classification methods.

V. CONCLUSION

The proposed GRU-FCN classification model shows that replacing the LSTM by a GRU enhances the classification accuracy without needing extra algorithm enhancements such as fine-tuning or attention algorithms. The GRU also has a smaller architecture that requires fewer computations than the LSTM. Moreover, the GRU-based model requires smaller number of trainable parameters, memory, and training time comparing to the LSTM-based models. Furthermore, the proposed GRU-FCN classification model achieves the performance of state-of-the-art models and has the highest average arithmetic ranking and the lowest mean per-class error (MPCE) through time series datasets classification of the UCR benchmark compared to the state-of-the-art models. Therefore, replacing the LSTM by GRU in the LSTM-FCN for univariate time series classification can improve the classification with smaller model architecture.

VI. ACKNOWLEDGMENT

We would like to thank Prof. Eamonn Keogh for his suggestions, comments, and ideas about our proposed work in this paper.

REFERENCES

- [1] J. D. Hamilton, *Time series analysis*. Princeton University Press, Princeton, NJ, 1994, vol. 2.
- [2] H. Sohn and C. R. Farrar, "Damage diagnosis using time series analysis of vibration signals," *Smart Materials and Structures*, vol. 10, no. 3, p. 446, 2001.
- [3] M. Gul and F. N. Catbas, "Statistical pattern recognition for structural health monitoring using time series modeling: theory and experimental verifications," *Mechanical Systems and Signal Processing*, vol. 23, no. 7, pp. 2192–2204, 2009.

TABLE VI: Wilcoxon signed-rank test on GRU-FCN and 10 benchmark model on the 85 datasets from UCR benchmark [14].

	<i>FCN</i>	<i>LSTM-FCN</i>	<i>ALSTM-FCN</i>	<i>ResNet</i>	<i>MCNN</i>	<i>MLP</i>	<i>COTE</i>	<i>DTW</i>	<i>PROP</i>	<i>BOSS</i>	<i>TSBF</i>	<i>ED</i>
GRU-FCN	3.44E-10	4.95E-03	4.00E-02	2.53E-11	1.05E-12	1.43E-13	1.25E-08	1.23E-14	1.58E-11	4.37E-10	2.77E-12	2.93E-15
FCN		4.37E-09	8.58E-08	1.68E-01	9.31E-10	1.12E-09	1.85E-02	3.49E-12	1.31E-07	8.02E-04	1.10E-07	7.07E-13
LSTM-FCN			7.45E-01	2.24E-09	1.40E-11	6.09E-13	1.03E-06	2.35E-14	5.72E-11	2.85E-9	6.40E-13	1.08E-14
ALSTM-FCN				1.40E-07	1.02E-11	8.35E-12	2.33E-07	1.55E-13	7.95E-11	4.71E-09	3.30E-12	4.73E-14
ResNet					6.28E-09	1.79E-08	2.46E-01	9.32E-13	1.76E-06	1.28E-03	1.56E-07	1.11E-13
MCNN						4.35E-05	4.77E-08	5.76E-05	6.10E-04	1.20E-06	7.72E-06	2.18E-04
MLP							7.04E-05	7.28E-01	7.13E-01	1.08E-03	5.70E-03	3.25E-04
COTE							1.62E-06	2.28E-06	7.74E-05	1.08E-03	3.59E-04	3.22E-07
DTW									2.05E-01	2.37E-07	1.80E-04	2.13E-03
PROP										8.82E-03	5.13E-01	3.14E-02
BOSS											3.18E-02	7.02E-10
TSBF												6.65E-08

- [4] Z. Wang, W. Yan, and T. Oates, "Time series classification from scratch with deep neural networks: a strong baseline," in *Neural Networks (IJCNN), 2017 International Joint Conference on*. IEEE, 2017, pp. 1578–1585.
- [5] F. Karim, S. Majumdar, H. Darabi, and S. Chen, "LSTM fully convolutional networks for time series classification," *IEEE Access*, vol. 6, pp. 1662–1669, 2018.
- [6] A. Amei, W. Fu, and C.-H. Ho, "Time series analysis for predicting the occurrences of large scale earthquakes," *International Journal of Applied Science and Technology*, vol. 2, no. 7, 2012.
- [7] J. Rotton and J. Frey, "Air pollution, weather, and violent crimes: concomitant time-series analysis of archival data," *Journal of Personality and Social Psychology*, vol. 49, no. 5, p. 1207, 1985.
- [8] E. Keogh and C. A. Ratanamahatana, "Exact indexing of dynamic time warping," *Knowledge and Information Systems*, vol. 7, no. 3, pp. 358–386, 2005.
- [9] P. Schäfer, "The BOSS is concerned with time series classification in the presence of noise," *Data Mining and Knowledge Discovery*, vol. 29, no. 6, pp. 1505–1530, 2015.
- [10] M. G. Baydogan, G. Runger, and E. Tuv, "A bag-of-features framework to classify time series," *IEEE Transactions on Pattern Analysis and Machine Intelligence*, vol. 35, no. 11, pp. 2796–2802, 2013.
- [11] J. Lines and A. Bagnall, "Time series classification with ensembles of elastic distance measures," *Data Mining and Knowledge Discovery*, vol. 29, no. 3, pp. 565–592, 2015.
- [12] A. Bagnall, J. Lines, J. Hills, and A. Bostrom, "Time-series classification with COTE: the collective of transformation-based ensembles," *IEEE Transactions on Knowledge and Data Engineering*, vol. 27, no. 9, pp. 2522–2535, 2015.
- [13] Z. Cui, W. Chen, and Y. Chen, "Multi-scale convolutional neural networks for time series classification," *arXiv preprint arXiv:1603.06995*, 2016.
- [14] Y. Chen, E. Keogh, B. Hu, N. Begum, A. Bagnall, A. Mueen, and G. Batista. (2015, July) The UCR time series classification archive. [Online]. Available: http://www.cs.ucr.edu/~eamonn/time_series_data/
- [15] J. Chung, C. Gulcehre, K. Cho, and Y. Bengio, "Empirical evaluation of gated recurrent neural networks on sequence modeling," *arXiv preprint arXiv:1412.3555*, 2014.
- [16] Y. LeCun, B. Boser, J. S. Denker, D. Henderson, R. E. Howard, W. Hubbard, and L. D. Jackel, "Backpropagation applied to handwritten zip code recognition," *Neural Computation*, vol. 1, no. 4, pp. 541–551, 1989.
- [17] Y. LeCun and Y. Bengio, "Convolutional networks for images, speech, and time series," in *The Handbook of Brain Theory and Neural Networks*. MIT Press, 1995, pp. 255–258.
- [18] I. Goodfellow, Y. Bengio, A. Courville, and Y. Bengio, *Deep Learning*. MIT press Cambridge, 2016, vol. 1.
- [19] S. Ioffe and C. Szegedy, "Batch normalization: Accelerating deep network training by reducing internal covariate shift," *arXiv preprint arXiv:1502.03167*, 2015.
- [20] V. Nair and G. E. Hinton, "Rectified linear units improve restricted Boltzmann machines," in *Proceedings of the 27th International Conference on Machine Learning (ICML-10)*, 2010, pp. 807–814.
- [21] (2019) Keras recurrent layers documentation. [Online]. Available: <https://keras.io/layers/recurrent/>
- [22] Y.-L. Boureau, J. Ponce, and Y. LeCun, "A theoretical analysis of feature pooling in visual recognition," in *Proceedings of the 27th international conference on machine learning (ICML-10)*, 2010, pp. 111–118.
- [23] K. He, X. Zhang, S. Ren, and J. Sun, "Delving deep into rectifiers: surpassing human-level performance on imagenet classification," in *Proceedings of the IEEE International Conference on Computer Vision*, 2015, pp. 1026–1034.
- [24] C. Gulcehre, M. Moczulski, M. Denil, and Y. Bengio, "Noisy activation functions," in *International Conference on Machine Learning*, 2016, pp. 3059–3068.
- [25] X. Glorot and Y. Bengio, "Understanding the difficulty of training deep feedforward neural networks," in *Proceedings of the Thirteenth International Conference on Artificial Intelligence and Statistics*, 2010, pp. 249–256.
- [26] F. Chollet *et al.*, "Keras," <https://keras.io>, 2015.
- [27] D. P. Kingma and J. Ba, "Adam: A method for stochastic optimization," *arXiv preprint arXiv:1412.6980*, 2014.
- [28] N. M. Nasrabadi, "Pattern recognition and machine learning," *Journal of Electronic Imaging*, vol. 16, no. 4, p. 049901, 2007.
- [29] M. Abadi, A. Agarwal, P. Barham, E. Brevdo, Z. Chen, C. Citro, G. S. Corrado, A. Davis, J. Dean, M. Devin, S. Ghemawat, I. Goodfellow, A. Harp, G. Irving, M. Isard, Y. Jia, R. Jozefowicz, L. Kaiser, M. Kudlur, J. Levenberg, D. Mané, R. Monga, S. Moore, D. Murray, C. Olah, M. Schuster, J. Shlens, B. Steiner, I. Sutskever, K. Talwar, P. Tucker, V. Vanhoucke, V. Vasudevan, F. Viégas, O. Vinyals, P. Warden, M. Wattenberg, M. Wicke, Y. Yu, and X. Zheng, "TensorFlow: Large-scale machine learning on heterogeneous systems," 2015, software available from tensorflow.org. [Online]. Available: <https://www.tensorflow.org/>
- [30] Y.-S. Jeong, M. K. Jeong, and O. A. Omitaomu, "Weighted dynamic time warping for time series classification," *Pattern Recognition*, vol. 44, no. 9, pp. 2231–2240, 2011.
- [31] Y. Sasaki *et al.*, "The truth of the f-measure," *Teach Tutor mater*, vol. 1, no. 5, pp. 1–5, 2007.
- [32] D. M. Powers, "Evaluation: from precision, recall and f-measure to roc, informedness, markedness and correlation," 2011.
- [33] J. Demšar, "Statistical comparisons of classifiers over multiple data sets," *Journal of Machine Learning Research*, vol. 7, no. Jan, pp. 1–30, 2006.
- [34] T. Pohlert, "The pairwise multiple comparison of mean ranks package (PMCMR)," *R Package*, vol. 27, 2014.
- [35] R. Woolson, "Wilcoxon signed-rank test," *Wiley encyclopedia of clinical trials*, pp. 1–3, 2007.
- [36] D. Rey and M. Neuhäuser, "Wilcoxon-signed-rank test," *International encyclopedia of statistical science*, pp. 1658–1659, 2011.
- [37] R. Lowry, "Concepts and applications of inferential statistics," 2014.



Nelly Elsayed is a PhD candidate in Computer Engineering at the School of Computing and Informatics, University of Louisiana at Lafayette. She received her Bachelor degree in Computer Science at Alexandria University in 2010 and she was ranked the First on Computer Science Class. She received two Masters degrees, the first in Computer Science in 2014 at Alexandria University and the second in Computer Engineering in 2017 at University of Louisiana at Lafayette. She is an honor member in the national society of leadership and the the honor

society Phi Kappa Phi. Her major research interests are in machine learning, deep learning, artificial intelligence, convolutional recurrent neural networks, bio-inspired computations, and quantum computing.



Anthony S. Maida is associate professor and graduate coordinator for computer science and computer engineering at School of Computing and Informatics, University of Louisiana at Lafayette. He received this BA in Mathematics in 1973, Ph.D. in Psychology in 1980, and Masters Degree in Computer Science in 1981, all from the University of Buffalo. He has done two Post Doctoral degrees at Brown University and the University of California, Berkeley. He was a member of the computer science faculty at the Penn State University from 1984 through 1991.

He has been a member of a Center for Advanced Computer Studies and School of Computing and informatics at the University of Louisiana at Lafayette from 1991 to the present. His research interests are: intelligent systems, neural networks, recurrent neural networks and brain simulation.



Magdy Bayoumi is department head and professor at the Electrical Engineering Department, University of Louisiana at Lafayette. He was the Director of CACS, 1997 2013 and Department Head of the Computer Science Department, 2000-2011. He has been a faculty member in CACS since 1985. He received B.Sc. and M.Sc. degrees in Electrical Engineering from Cairo University, Egypt; M.Sc. degree in Computer Engineering from Washington University, St. Louis; and Ph.D. degree in Electrical Engineering from the University of Windsor,

Canada. He is on the IEEE Fellow Committee and he was on the IEEE CS Fellow Committee. His research interests are: technology, data processing, management, energy and security.